LIMNOLOGY and OCEANOGRAPHY

ASLO

Limnol. Oceanogr. 66, 2021, 3887–3900

doi: 10.1002/lno.11927

Hydraulic and biological controls of biofilm nitrogen uptake in gravel-bed streams

Christine Anlanger,[1,2*] **Ute Risse-Buhl**,[2] **Daniel von Schiller**,[3] **Christian Noss**,[1,4] **Markus Weitere**,[2] **Andreas Lorke**[1]

[1]Institute of Environmental Sciences, University of Koblenz-Landau, Landau, Germany
[2]Department of River Ecology, Helmholtz Centre for Environmental Research – UFZ, Magdeburg, Germany
[3]Department of Evolutionary Biology, Ecology and Environmental Sciences, Faculty of Biology, University of Barcelona, Barcelona, Spain
[4]Federal Waterways Engineering and Research Institute, Karlsruhe, Germany

Abstract

Epibenthic biofilms are important in regulating nitrogen (N) fluxes in stream ecosystems. The efficiency of the regulation is controlled by hydraulic and biological processes and their interactions. However, knowledge on the underlying physical and biological processes, their controlling parameters, and interactions in stream ecosystems is still limited. To analyze the relative importance of hydraulic and biological controls on biofilm N uptake, we measured turbulence, biofilm N uptake using a stable isotope tracer, and biofilm biomass in two gravel-bed streams with contrasting nutrient concentrations for two seasons. We found high within-stream variability in biofilm areal N uptake and uptake velocity, which exceeded variability between streams and seasons by 60% and 30%, respectively. Sixty-four percent of the within-stream variability in uptake velocity was explained by hydraulic mass transfer and biofilm characteristics, which were described in terms of the turbulent dissipation rate and the biofilm biomass, respectively. We show that surface renewal theory based on scales of the smallest turbulent eddies can be used to estimate transfer velocities at the sediment–water interface and can be extrapolated to larger scales by spatial averaging. Our results improved the mechanistic understanding of the processes regulating biofilm N uptake at small scale which contributes to the understanding of ecosystem functioning in low-order streams and supports upscaling to larger spatiotemporal scales along stream networks.

Input of dissolved inorganic nitrogen (N) to aquatic ecosystems has been increasing globally as a result of human activities, particularly agricultural land use and discharge from wastewater treatment plants (Galloway et al. 2008; Seitzinger et al. 2010). Streams constitute biogeochemical reactors that can take up, store, and transform N during downstream transport. Low-order streams have an important role in N cycling, in particular during seasons of high biological activity (Alexander et al. 2007; Marcé et al. 2018). The large ratio of solid substrate area to water volume promotes the dominance of biofilm-dwelling microbes over planktonic microbes and most N cycling is driven by epibenthic biofilms (Newbold et al. 1982; Sabater et al. 2002; Tank et al. 2018). The functional significance of biofilms depends on their attributes (e.g., biofilm composition and morphology), as well as nutrient supply from the water column (Battin et al. 2007).

Besides a number of chemical and biological processes, stream flow can be a key controlling factor of biofilm N uptake by mediating mass transfer across the concentration boundary layer at the streambed (Kim et al. 1992; Larned et al. 2004; Tomasek et al. 2018). Mass transfer can be a limiting step in nutrient uptake, particularly at low flow velocity, while at higher velocity uptake often becomes biologically limited (Nepf 2011). Moreover, hydraulics may indirectly affect N uptake and storage by altering biofilm architecture (Stoodley et al. 1998; Risse-Buhl et al. 2017) and biomass (Biggs and Thomsen 1995; Stevenson 1996) and probably also N transfer within the microbial biofilm food web (Weitere et al. 2018; Risse-Buhl et al. 2020*a*). Biofilms growing on surfaces exposed to high bottom shear stress, caused by high flow velocity and strong turbulence, have lower biomass than biofilms growing under low shear stress (Biggs and Thomsen 1995). However, a mechanistic understanding of the processes that regulate the relative importance of physical and biological processes that control N uptake and its spatial variability is limited.

*Correspondence: christine.anlanger@ufz.de

Additional Supporting Information may be found in the online version of this article.

Epibenthic biofilms develop to a great extent in the protective cover of the viscous sublayer (Vogel 1994), that is, the near-bed layer at which the flow becomes laminar and frictional force is governed by the viscosity of water rather than turbulent eddies. Biofilms also interact with near-bed flow by increasing bed roughness (Nikora et al. 2002). In order to sustain increased drag forces, biofilm organisms with specific morphologies that promote attachment and association to solid surfaces are favored (Biggs and Thomsen 1995; Battin et al. 2003*a*). Within the viscous sublayer, a concentration gradient may develop creating a diffusive boundary layer, where mass transport is controlled by molecular diffusion (i.e., diffusive boundary layer). The vertical extent of the viscous and diffusive boundary layers scales with the size of the smallest turbulent eddies (i.e., Kolmogorov microscale) and depends on the dissipation rate of the turbulent kinetic energy (ε; Lorke and Peeters 2006). Mass transfer across the boundary layer is commonly described in terms of a mass transfer velocity. The uptake rate at the streambed is commonly expressed as an uptake velocity, which is the areal uptake rate divided by in-stream concentration. The overall uptake velocity can be decomposed into a hydraulically controlled mass transfer velocity toward the streambed and a biologically mediated uptake velocity at the bed, with the mass transfer velocity imposing an upper limit for the overall uptake velocity (Grant and Marusic 2011). Grant et al. (2018*b*) defined uptake efficiency as the ratio of the overall uptake velocity and the mass transfer velocity. The mass transfer velocity depends on the near-bed turbulence and is related to the turbulent dissipation rate by the surface renewal model (Lorke and Peeters 2006; O'Connor and Hondzo 2008). Grant et al. (2018*a*) applied the surface renewal model for analyzing a large data set on reach-scale N uptake using ε estimated from bulk stream characteristics (bed slope and mean flow depth). The bulk approach is based on the assumption of a homogenous distribution of turbulence within stream reaches. In gravel-bed streams, near-bed flows are complex, three-dimensional, and heterogeneous, resulting from broad size distributions of roughness elements (Lamarre and Roy 2005; Noss and Lorke 2016). Therefore, ε near the streambed vary over several orders of magnitude and result in high variability of mass transfer at small spatial scales.

In addition to the heterogeneity at the microscale, near-bed flow and turbulence vary among larger hydromorphologic habitats. Gravel-bed streams are composed of alternating riffle and pool sections, which differ in water depth, flow velocity, water surface, and bed slope (Montgomery and Buffington 1997). Mean flow velocity and turbulence are higher in riffles, which promote higher areal N uptake by stream biofilms (Peipoch et al. 2016; Risse-Buhl et al. 2020*b*). In view of the small-scale mechanistic basis of the surface renewal model, it remains questionable to what extent and at which spatial scales it can be applied to quantify the mass transfer velocity in heterogeneous streams. It is thus vital to understand the mechanisms at smaller scales and if these processes can be scaled up to larger scales by applying bulk metrics. Moreover, a mechanistic understanding and quantification of mass transfer limitation allows disentangling physical and biological controls on nutrient uptake in epibenthic biofilms.

Based on measurements of near-bed turbulence and biofilm N uptake in two rivers, we analyzed how locally variable flow conditions affect biofilm N uptake in gravel-bed streams. To cover the broad range of different hydraulic conditions within the streams, we deployed a nested sampling approach starting with high-resolution near-bed velocity measurements at the microscale and expanding to the mesoscale with distinct hydromorphological habitats. The hydraulic measurements were aligned with microscale measurements of biofilm N uptake rates using stable isotope (^{15}N) tracer additions and biofilm sampling. We used the surface renewal model to estimate mass transfer velocities and to test the hypothesis that locally variable transfer velocities can be averaged to larger scales and estimated from bulk stream metrics. We further evaluated the relative importance of mass transfer and biological uptake and hypothesized that the biological component of the uptake velocity is related to biofilm biomass. Consequently, we expected that the relative importance of biological controls on N uptake depends on environmental conditions that affect biofilm biomass. Therefore, all measurements were conducted in two streams with contrasting nutrient concentrations and at two seasons. With this multidisciplinary approach, we ultimately aim at improving our mechanistic understanding of environmental controls on N uptake at the microscale and their superposition to the scale of hydromorphological habitats.

Methods

Study sites and sampling approach

Measurements were conducted in two streams, Kalte Bode and Selke streams, which are located in the Bode catchment in the Harz Mountains in Central Germany (Fig. 1; Table 1). The catchments are part of the Terrestrial Environmental Observatories, a long-term monitoring program (Wollschläger et al. 2017). Both streams are coarse-grained mountainous streams exhibiting a natural flow regime with almost no anthropogenic influences except of some modifications for bank stabilization. The Kalte Bode comprises sediments ranging from fine gravel to boulders (2–630 mm) and the Selke additionally comprises sand (0.063–2 mm). At the mesoscale with spatial scales of $\sim 10^0$ m (Frissell et al. 1986), we divided the study reaches into distinct hydromorphological habitats (i.e., riffle and pool; Montgomery and Buffington 1997). Gauging stations close to the study sites provided daily discharge data for the periods 1921–2015 (Selke) and 1951–2014 (Kalte Bode; Table 1). Bank vegetation of the Kalte Bode consists of a coniferous forest at the right bank and pasture with sparsely distributed bushes and deciduous trees on the left bank,

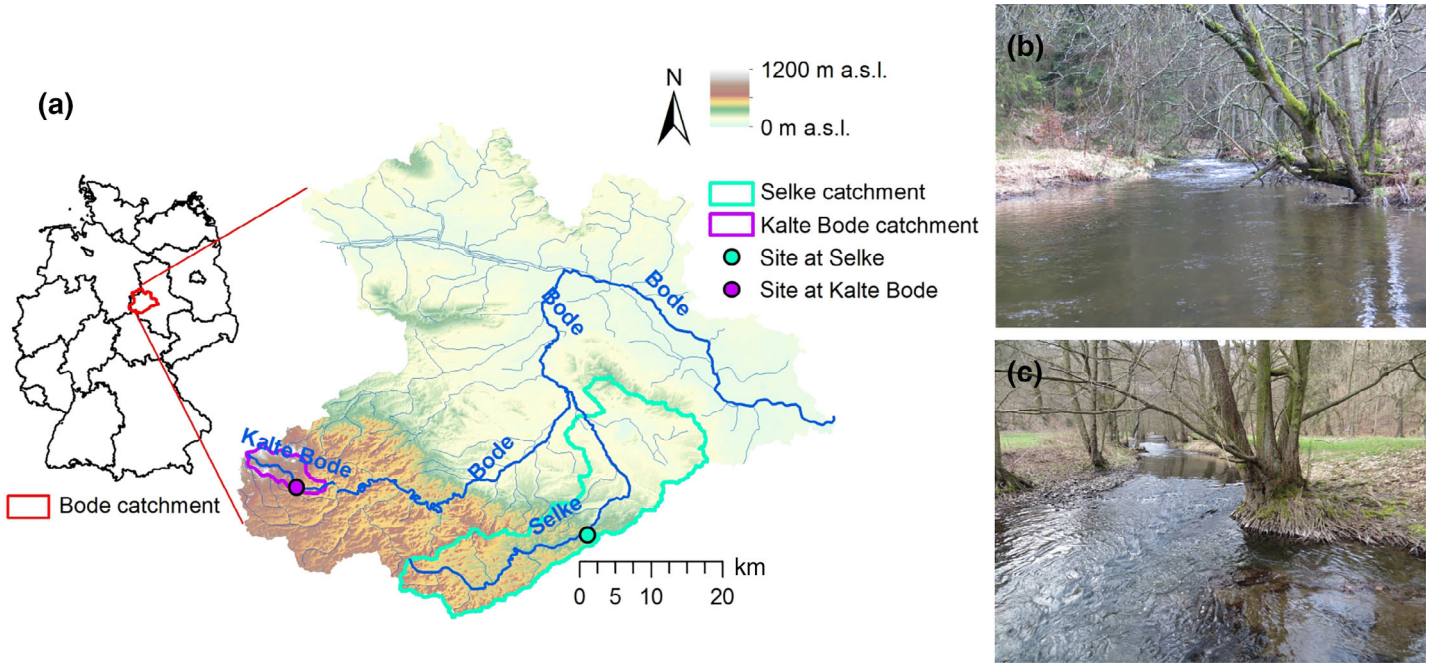

Fig. 1. Location (**a**) and pictures of the study sites at the Kalte Bode (**b**) and Selke (**c**) streams situated in the Bode catchment in the Harz Mountains (Germany).

Table 1. Location and hydraulic characteristics of the study reaches at the Kalte Bode and Selke streams.

					Study reach		
Stream	Coordinates	Catchment area (km^2)	Mean discharge ($m^3\ s^{-1}$)	Baseflow ($m^3\ s^{-1}$)	Length (m)	Mean width (m)	Mean water level slope (%)
Kalte Bode	N 51°44′33″, E 10°42′09″	26	0.72	0.18	580	7.2	0.82
Selke	N 51°41′11.5″, E 10°15′34″	184	1.52	0.24	490	7.3	0.39

whereas the stream banks of the Selke are lined with a sparse row of deciduous trees. The selected stream reaches had similar length and width, but differed in the mean water level slope and the mean discharge (Table 1).

In total, we conducted four measurement campaigns: one in summer 2014 and one in spring 2015 in each stream, respectively. We aimed at performing measurements and experiments during similar hydrological conditions (i.e., close to baseflow). During each campaign, measurements of near-bed hydraulics at the spot-scale (approximately 7 ± 3 cm^2, which corresponds to the mean and standard deviation of the biofilm sampling area) were followed by a stable isotope (^{15}N) tracer addition experiment and subsequent sampling of biofilms for stable isotope analyses. During the tracer addition, ^{15}N-NH_4^+ was added to increase the ^{15}N : ^{14}N ratio of available N in stream water (see also Risse-Buhl et al. 2020*b*). Assimilatory NH_4^+ uptake was quantified by the flux of ^{15}N tracer into the biofilms, which was calculated as ^{15}N enrichment over time after subtracting natural isotope abundance. Riffles and pools were visually distinguished by undulations of the water surface. The measurement spots were randomly distributed within riffles and pools (with $2 \le n \le 12$ and mean $n = 8.1$) in each habitat. Variations in the amount of sampling spots resulted from a smaller number of measurements and samples during the first campaign (Selke summer) and from individual variations in the number of hydraulic measurements and biofilm samples which restricted our paired sampling approach. Some habitats along the experimental reach could not be sampled because of inaccessibility. In total, three riffles and up to five pools were sampled in Kalte Bode and four riffles and three pools were sampled in Selke.

For both seasons, Kalte Bode had lower soluble reactive phosphorus (SRP) concentrations than Selke (Table 2). Considering the ratio of total dissolved nitrogen (DIN; sum of nitrate [NO_3^-] and ammonium [NH_4^+]) and SRP concentrations, Kalte Bode can be referred to as nutrient poorer and Selke as nutrient richer 2. Spring was the season with the highest photosynthetic active radiation in the stream channel, in

particular at Selke. Water temperature was around 10°C during all field campaigns, except for Selke in summer, when it reached 17°C (Table 2).

Measurements and data analysis

Physical stream characteristics at the mesoscale

The lengths (m) and mean widths (W, m) of the hydromorphological habitats were determined with a tape measure. The vertical water level difference between habitats was used to estimate the mean water level slope (S, %). For Selke, mean water depth (H, m) of each habitat and the reach were estimated from topographical data provided by the local water authority for a daily mean discharge of 0.26 ± 0.08 m^3 s^{-1} (mean ± standard deviation). In Kalte Bode, we conducted a topographical survey using an electronic tachymeter with differential global positioning system and global navigation satellite system rover (Trimble S8 total station and Trimble R8 GNSS System, Trimble) during a mean daily discharge of 0.57 ± 0.07 m^3 s^{-1} and thus, also in the range between baseflow and mean discharge. Reach-scale mean values of the turbulent dissipation rate (ε_{bulk}, W kg^{-1}) were estimated for each habitat from bulk parameters as:

$$\varepsilon_{bulk} = (gRS)^{2/3} H^{-1}, \quad (1)$$

where R is the hydraulic radius ($R = HW(2H + W)^{-1}$, m) and g (m s^{-2}) is the gravitational acceleration (Moog and Jirka 1999).

Hydraulic measurements and analyses

Time series of the three-dimensional flow velocities were measured at approximately 60 spots per campaign, using a multistatic acoustic Doppler velocity profiler (Vectrino II, Nortek AS) at a sampling frequency of 64 Hz. We chose the maximum vertical profiling range of the instrument (35 mm) with a resolution of 1 mm and set the profiling range such that the lowermost velocity measurement coincided with the sediment–water interface. However, reliable turbulence measurements of the Vectrino II can be expected only around a so-called sweet spot (Brand et al. 2016; Koca et al. 2017), which in our measurements was located 2.3 cm above the sediment. Therefore, we restricted our analysis to that single measurement height. A sampling duration of 20 min was chosen, which is sufficiently long for providing accurate characteristics of turbulence and facilitates spectral analysis of turbulent velocity fluctuations (Buffin-Bélanger and Roy 2005). Raw data were filtered with a threshold of 15 dB for the signal-to-noise ratio and of 70% for signal correlation. The filtered velocities were despiked using the method described by Goring and Nikora (2002), modified by Wahl (2003). Outliers were replaced by the nearest valid data points, and the resulting velocity vectors were rotated such that u, v, and w (m s^{-1}) denote the longitudinal, transversal, and vertical component of the mean flow velocity vector, respectively.

Measurement noise was removed from the final velocities by low-pass filtering, while the cutoff frequency of the filter was estimated from power spectra of each velocity time series and each velocity component. Noise was identified in the spectra as the breakpoint in spectral slope, where the spectra flattened at high frequencies. The Reynolds averaged longitudinal flow velocity ($\overline{u}$, m s^{-1}) was estimated as the arithmetic mean of all velocity measurements (u_i, m s^{-1}). The turbulent kinetic energy (E, m^{2}s^{-2}) was estimated from turbulent velocity fluctuations (u', v', w'; m s^{-1}), which were obtained by subtracting the mean values from measured (instantaneous) velocity components:

$$E = 0.5\left(\overline{u'^2} + \overline{v'^2} + \overline{w'^2}\right), \quad (2)$$

where the overbar denotes temporal averaging. The mass transfer velocity (k, m s^{-1}) was estimated according to Katul and Liu (2017):

$$k = \alpha_1 (\varepsilon\nu)^{0.25} Sc^{-0.5}, \quad (3)$$

where Sc is the Schmidt number, which is the ratio of the kinematic viscosity (ν, m^2 s^{-1}) depending on water temperature and the molecular diffusion coefficient of ammonium in water (1.86×10^{-9} m^2 s^{-1}). α_1 is a dimensionless scaling factor, which

Table 2. Nutrient concentrations, including nitrate (NO_3^-), ammonium (NH_4^+), soluble reactive phosphorus (SRP), photosynthetic active radiation (PAR), temperature (T), dissolved oxygen concentration (DO), pH and, specific electrical conductivity (C) for both streams and seasons. DIN : SRP denotes the molar ratio of dissolved inorganic nitrogen (DIN, sum of NO_3^- and NH_4^+) and SRP. All data are presented as mean with standard deviation in brackets during the tracer addition experiment. *n* is the number of observations. PAR, T, DO, pH, and C were measured at a 15 min interval.

		NO_3^-	NH_4^+	SRP	DIN : SRP	PAR	T	DO	pH	C
		μg N L^{-1}		μg L^{-1}		mol m^{-2} d^{-1}	°C	mg L^{-1}		μS cm^{-1}
Stream	Season	$n = 24$	$n = 21$	$n = 21$						
Kalte Bode	Summer	490 (31)	10 (1)	3 (0)	75	10.4 (1.3)	10.2 (0.7)	10.6 (0.2)	7.4 (0.1)	89 (2)
	Spring	661 (27)	68 (14)	3 (0)	110	13.2 (1.4)	10.2 (1.4)	10.7 (0.4)	7.5 (0.1)	92 (2)
Selke	Summer	559 (20)	45 (5)	47 (1)	6	4.3 (2.5)	17.2 (0.8)	8.7 (0.3)	8.0 (0.1)	496 (11)
	Spring	1170 (32)	57 (4)	11 (1)	50	12.9 (2.9)	11.3 (1.9)	10.5 (0.8)	8.1 (0.3)	365 (15)

depends on the distance to the interface at which ε has been estimated (Lorke and Peeters 2006) and was chosen to be 0.4 (Lorke et al. 2019). Details on the choice of α_1 are highlighted in the discussion. The turbulent dissipation rate (ε, W kg^{-1}) was estimated from fitting power spectra of vertical velocity fluctuations to theoretical spectra within the inertial subrange (inertial dissipation technique; Bluteau et al. 2011). Furthermore, ε at the meso and reach-scale (ε_S, W kg^{-1}) was calculated for each habitat and reach in both streams and for both seasons:

$$\varepsilon_S = 10^{\frac{1}{n}\sum \log(\varepsilon_i)}, \quad (4)$$

with n being the number of hydraulic measurements conducted in a habitat or reach and ε_i denoting dissipation estimates obtained at different spots i within the respective habitat or reach. $\varepsilon_{\text{bulk}}$ (Eq. 1) and ε_S (Eq. 4) were used to calculate k for the mesoscale according to Eq. 3 resulting in k_{bulk} (m s^{-1}) and k_ε (m s^{-1}) for each habitat, respectively.

After measuring flow velocity, the sampling location was marked with a label positioned on the streambed. A macrophotograph was taken from each position, where a laser pointer highlighted the precise location of the flow measurement on the bed. The photograph was used to identify the sampling location for later biofilm sampling.

Tracer addition, sampling, and analyses

At each stream and season, we conducted a 24-h addition of ^{15}N-labeled ammonium chloride ($^{15}NH_4Cl$, 99% ^{15}N enriched, reactive tracer) and sodium bromide (NaBr, conservative tracer, see also Risse-Buhl et al. 2020*b*). The tracer addition followed an adaptation of the protocol established for the Lotic Intersite Nitrogen eXperiment project (Mulholland et al. 2000). Stable isotope values of N are reported as δ^{15}N (‰) according to $\left[\left(R_{\text{sample}}/R_{\text{standard}}\right)-1\right]\times 1000$ where R_{sample} is the ^{15}N : ^{14}N ratio in the sample and R_{standard} is the international standard of ^{15}N : ^{14}N in air. The tracer solution was added with a peristaltic pump (Watson-Marlow) located 250 m (Kalte Bode summer and spring), 136 m (Selke summer), and 166 m (Selke spring) upstream of the study reaches to ensure complete lateral and vertical mixing (Day 1977). The amount of ^{15}N tracer and the pump flow rate were set to achieve a target ^{15}N enrichment of 1000‰ in the water column at the addition site. Although some amount of the tracer was taken up along the mixing section, isotopic ratio was still traceable in the experimental reach. To verify plateau conditions during each addition, an autosampler (AWS 2002, Endress+Hauser AG Reinach) collected water samples for Br^- analysis every 2 h supplemented by manual water collection at shorter time intervals (i.e., minimum 2 min) after start and stop of each addition at the upstream and downstream end of the study reaches. Plateau enrichment was achieved after 2 h maximum, and after 19 h we started the sampling of biofilms and stream water, which was completed within 4–5 h. For the calculation of fluxes, water was sampled at each habitat and analyzed for concentrations of NH_4^+-N, NO_3^--N, SRP, $^{15}NH_4^+$, and Br^- 1 d prior to tracer addition for background characterization and during the plateau. Background ^{15}N was determined in duplicated epilithic biofilm samples collected at three habitats located within the study reaches 1 d prior to the tracer addition. Biofilms were sampled by removing the stone from the streambed. The biofilms were removed by brushing the stone's surface twice with a sterile toothbrush and rinsing with 30 mL of sterile filtered stream water (prefiltered through GF/F and sterile filtered through Cellulose-Acetate membrane, pore size 0.2 μm, Sartorius). Finally, the area covered by the removed biofilm was projected to a tinfoil. The area of each tinfoil piece was quantified with the software Fiji (Schindelin et al. 2012).

Stream water NH_4^+-N, NO_3^--N, and SRP concentrations were analyzed by standard procedures as described in Risse-Buhl et al. (2017). Concentrations of Br^- were measured in untreated samples by inductively coupled plasma mass spectrometry (ICP-MS Triple Quadrupole, Agilent Technologies).

Samples for ^{15}N analysis in water were acidified to a pH of 2 and shipped to the Boston University Stable Isotope Laboratory, where δ^{15}N in NH_4^+ was determined using a Finnigan Delta S mass spectrometer (Thermo Fisher Scientific), following NH_4^+ diffusion under alkaline conditions (Holmes et al. 1998). For the analysis of ^{15}N in biofilms, samples were dried at 60°C for 48 h, weighed for dry mass, grounded, and packed in tin capsules before analyzing δ^{15}N and N content using a Flash 2000 HT elemental analyzer coupled via a ConFlo IV interface to a Delta V Advantage isotope ratio mass spectrometer (all Thermo Fisher Scientific).

Water temperature, dissolved oxygen concentration, pH, and specific electrical conductivity were measured during each field campaign at the upstream station of the study reaches using a multiparameter probe (EXO2, YSI Incorporated). Four to five light loggers (HOBO, Pendant Temperature/Light Data Logger UA-002-64, Onset Computer Corporation) were deployed near each stream in 1.0–2.5 m height to measure light intensity, which was further converted to daily photosynthetic active radiation (see also Risse-Buhl et al. 2017).

Calculation of biofilm N uptake metrics

The sampling described above provided all parameters necessary to estimate the uptake of NH_4^+ by biofilms (Mulholland et al. 2000; von Schiller et al. 2007; Ribot et al. 2013). First, the amount of tracer in the biofilm ($^{15}N_{\text{Biof}}$, mg ^{15}N m^{-2}) was calculated as:

$$^{15}N_{\text{Biof}} = N_{\text{Biof}}\left(MF_{\text{plateau}} - MF_{\text{background}}\right), \quad (5)$$

where N_{Biof} (mg N m^{-2}) is the biofilm N content and MF_{plateau} and $MF_{\text{background}}$ are the molar fractions of ^{15}N in biofilm at plateau and background conditions, respectively. Molar fractions were calculated as

Table 3. Spatial average of hydraulic parameters, N uptake parameters and biofilm dry mass (DM, g m^{-2}) for each stream and season. The parameters include discharge (*Q*, $m^3\ s^{-1}$), near-bed flow velocity ($\overline{u}$, $m\ s^{-1}$), turbulent kinetic energy (*E*, $10^{-3}\ m^2\ s^{-2}$), dissipation rate of the turbulent kinetic energy (ε, $10^{-3}\ W\ kg^{-1}$), mass transfer velocity (*k*, $m\ s^{-1}$), biofilm areal N uptake (U_{Biof}, $mgN\ m^{-2}\ d^{-1}$), overall N uptake velocity (v_f, $10^{-4}\ m\ s^{-1}$), biofilm N uptake velocity (v_{bed}, $10^{-4}\ m\ s^{-1}$), and N uptake velocity calculated from longitudinal tracer decline in the water column (v_{f_water}, $10^{-4}\ m\ s^{-1}$; values taken from Risse-Buhl et al. 2020*b*). v_{f_water} from the Selke stream is reported for comparison, despite a nonsignificant change of tracer concentration with distance negative values of v_{f_water} are set to zero. *n* is the number of observations. *n* for v_{bed} refers to the number of matching hydraulic measurements and biofilm samples and to the number of negative estimates of v_{bed}, that were excluded from further analyses as they do not match the model pre-requisites of Grant et al. (2018*a*). Discharge values were taken from a nearby gauging station (Q_st, $m^3\ s^{-1}$) and from tracer measurements (Q_tr, $m^3\ s^{-1}$) when available. All values, except for Q and v_{f_water} (upper and lower 95% confidence interval), are the spatial average over all sampling spots available (spatial average ± standard deviation). Angle brackets denote the spatial average.

		Hydraulic measurements					Tracer addition and biofilm sampling							Calculated from Eq. 8	
		n	Q_st	$\langle\overline{u}\rangle$	$\langle E\rangle$	$\langle\varepsilon\rangle$	$\langle k\rangle$	*n*	Q_st	Q_tr	$\langle$DM$\rangle$	$\langle U_{Biof}\rangle$	$\langle v_f\rangle$	v_{f_water}	*n*	$\langle v_{bed}\rangle$
Kalte Bode	Summer	64	0.33	0.14(0.09)	2.75(2.89)	2.65(4.62)	0.92(0.49)	66	0.36	0.22	19(18)	52(82)	1.20(1.90)	0.66(0.19–1.13)	61, 21	1.68(3.26)
	Spring	60	0.37	0.19(0.12)	4.75(5.37)	5.08(13.56)	1.08(0.55)	66	0.30	0.26	36(60)	172(253)	0.31(0.46)	0.52(0.01–1.02)	58, 5	0.36(0.60)
Selke	Summer	46	0.47	0.21(0.12)	5.16(4.89)	5.37(8.32)	1.25(0.52)	57	0.25	0.31	17(20)	17(16)	0.05(0.04)	0.32(0–1.58)	46, 0	0.05(0.05)
	Spring	59	1.16	0.34(0.12)	10.58(9.39)	10.77(14.29)	1.52(0.54)	67	0.61	0.77	30(38)	106(164)	0.21(0.32)	0(0–1.56)	57, 1	0.54(1.70)

$$MF = \frac{^{15}N}{^{15}N + ^{14}N} = \frac{\left(\frac{\delta^{15}N}{1000} + 1\right) \times 0.0036765}{1 + \left[\left(\frac{\delta^{15}N}{1000} + 1\right) \times 0.0036765\right]}. \quad (6)$$

We further quantified biofilm areal N uptake rate in form of NH_4^+ (U_{Biof}, mg N m^{-2} d^{-1}) according to:

$$U_{Biof} = \frac{^{15}N_{Biof}}{\left(\frac{^{15}N}{N_{flux}}\right)\delta t} \quad (7)$$

where $^{15}N_{flux}$ (mg ^{15}N s^{-1}) is the background corrected $^{15}NH_4^+$ flux in water at plateau conditions, N_{flux} (mg N s^{-1}) is the total NH_4^+ flux in water, and δt (s) is the time from start and stop of the tracer addition (i.e., 1 d). Discharge for flux calculations was determined based on the dilution data from the Br^- tracer collected in each habitat in close proximity to the biofilm samples.

Overall N uptake velocity (v_f, m s^{-1}) was estimated as U_{Biof} normalized by the local, ambient NH_4^+-N concentration in water collected together with Br^- samples. v_f can be decomposed in two parameters: the mass transfer velocity through the concentration boundary layer *k*, which is mediated by local hydraulic conditions, and the uptake velocity of the streambed v_{bed}, which is mediated by assimilation and denitrification processes of biofilms. Following Grant et al. (2018*a*), v_{bed} (m s^{-1}) was calculated as:

$$v_{bed} = \left(\frac{1}{v_f} - \frac{1}{k}\right)^{-1}, \quad (8)$$

and is further referred to biofilm uptake velocity. For details of the underlying model we refer to Grant et al. (2018*a*,*b*). The model assumes that the mass transfer *k* poses an upper limit to v_f and thus $k \geq v_f$. Negative values of v_{bed} resulting from Eq. 8 were excluded from subsequent statistical analysis. Negative values arise from measurement errors, and are most pronounced when variations of v_f are large (see also Fig. 1 in Grant et al. 2018*a*).

Statistical analyses

The relationships between (1) bulk hydraulic parameters (i.e., $\overline{u}$, *E*) and ε, *k*, biofilm dry mass, and U_{Biof}, (2) k_{bulk} and k_ε, (3) *k* and v_f, (4) biofilm dry mass and v_{bed}, and (5) measured v_f and v_f estimated from *k* and biofilm dry mass, were tested by linear regression analyses. Data used for regression analyses in (1), (4), and (5) were ln-transformed because residuals were not normally distributed (Shapiro–Wilk Test, Sigmaplot 13, Systat Software GmbH). In order to get the true factor distinguishing the parameters *k* and v_f (3; Fig. 4), we refrained from a ln-transformation despite residuals were not normally distributed. The regression equations of (4) were used to predict v_{bed} from dry mass for the spot-scale for each stream and season. We are aware of possible collinearity between v_{bed} and dry mass; however, the form and strength of this relationship may provide relevant information on the relative importance

of biological N uptake in front of hydraulic factors. Subsequently, v_f was calculated according to Eq. 8 from both, dry mass via the relationship to v_{bed} and k for each stream and season. Effects of the category "measurement campaign" on k_{bulk} and k_ε and statistical differences between riffles and pools for the spatial average within each habitat of hydraulic characteristics (i.e., $\langle\overline{u}\rangle$, $\langle E\rangle$, $\langle\varepsilon\rangle$, $\langle k\rangle$, angle brackets denote spatial averaging), uptake metrics (i.e., $\langle U_{Biof}\rangle$, $\langle v_{bed}\rangle$, $\langle v_f\rangle$), biofilm dry mass ($\langle DM\rangle$) and the mean ratio of v_f and k which can be referred to as uptake efficiency sensu Grant et al. (2018*a*) ($\langle v_f/k\rangle$) for each experiment were tested with an ANOVA on ranks, Dunn's method (Sigmaplot 13, Systat Software GmBH). All test results were regarded as statistically significant if $p<0.05$.

Results

Stream characteristics

Hydraulics

Discharge was slightly higher during the spring campaign at the Selke and also varied between the period of hydraulic measurements and subsequent tracer experiment in the Selke in summer and spring (Table 1). However, discharge during all measurements and experiments was within baseflow and mean discharge, therefore reflecting the predominant hydrological regime of both streams. $\langle\overline{u}\rangle$, $\langle E\rangle$, and $\langle\varepsilon\rangle$ were generally lower in Kalte Bode than in Selke. In both streams, these hydraulic parameters were approximately 50% lower in summer compared to spring. In contrast, $\langle k\rangle$ varied only slightly between streams and seasons and ranged from $0.92\times10^{-4}\,m\,s^{-1}$ in Kalte Bode in summer to $1.52\times10^{-4}\,m\,s^{-1}$ in Selke in spring (Table 3).

Hydraulic parameters were significantly higher in riffles than in pools for each stream and for both seasons (Table S1 in Supporting Information). In both streams, $\langle\overline{u}\rangle$ was approximately two times higher in riffles than in pools and $\langle E\rangle$ was up to five times higher in riffles than in pools. The difference in $\langle\varepsilon\rangle$ between riffles and pools was even larger: in Selke, $\langle\varepsilon\rangle$ was approximately 8 times higher in riffles than in pools, whereas in Kalte Bode it was 18 times higher. $\langle k\rangle$ was twice as high in riffles as in pools (Table S1 in Supporting Information).

All hydraulic spot-scale parameters were correlated across streams and seasons. E significantly explained the variance of ε and k by 86%, whereas $\overline{u}$ explained 44% and 45% of the variability of ε and k, respectively (Fig. S1 in Supporting Information).

The two different estimates of the turbulent dissipation rates obtained from spatial averaging of spot-scale measurements (ε_S, Eq. 4) and from bulk hydraulics (ε_D, Eq. 1) agreed well, and the corresponding mass transfer velocities k show a significant positive linear relationship ($R^2 = 0.90$, $p < 0.001$) with a slope of 0.97 (Fig. 2). As there was no statistically significant effect of measurement campaign on both, k_ε and k_{bulk} we did not differentiate between campaigns.

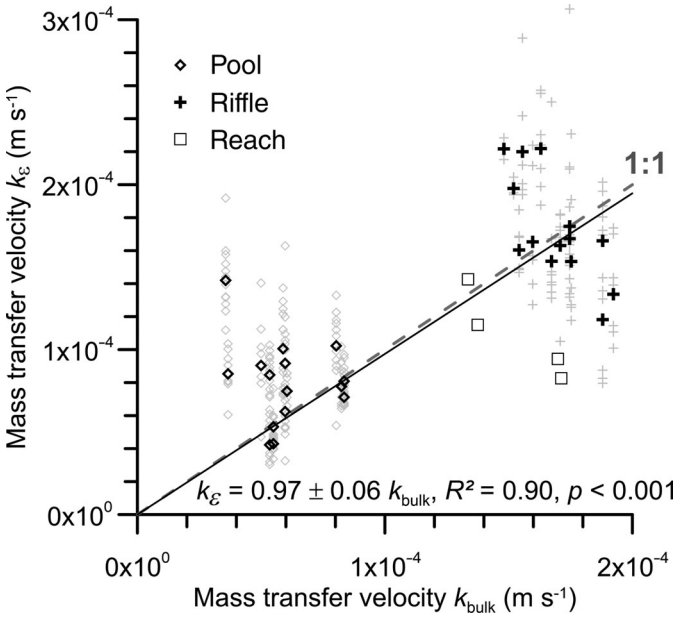

Fig. 2. Comparison of mass transfer velocities at the meso and reach-scale with k_ε calculated from ε_S (turbulent dissipation rates on the spot-scale and log-averaged for each habitat and reach) and k_{bulk} calculated from ε_{bulk} (turbulent dissipation rate calculated from stream bulk parameters). Black symbols show mass transfer velocities for hydromorphological habitats of each stream and season with different symbols marking riffles and pools. Gray symbols show mass transfer velocities measured at individual sampling spots within each habitat. The solid line shows the linear fit through the origin (regression equations including standard error of the slope and regression statistics are shown in the lower part of the panel) and the dashed gray line shows a 1 : 1 relationship.

Biofilm biomass and N uptake

Spatially averaged biofilm dry mass ($\langle DM\rangle$, angle brackets denote the spatial average) was similar between both streams, with higher values in spring than in summer (Table 1). All biofilm parameters showed high within-stream variability, with standard deviations of one to two times their mean values. $\langle DM\rangle$ tended to be lower in riffles than in pools for all streams and seasons, although the difference was only significant for Kalte Bode in spring and for Selke in summer (Table S2 in Supporting Information).

The spatially averaged biofilm areal N uptake rate ($\langle U_{Biof}\rangle$) was more than threefold (Kalte Bode) and sixfold (Selke) higher in spring than in summer. Spatially averaged, overall N uptake velocity ($\langle v_f\rangle$) in Kalte Bode was approximately four times higher in summer than in spring. For both seasons, $\langle v_f\rangle$ was lower in Selke than in Kalte Bode (Table 1). At Kalte Bode in spring, reach-scale N uptake velocity calculated from the decline of the isotope tracer in surface water (v_{f_water}) was within the range of $\langle v_f\rangle$ but v_{f_water} in summer was lower than $\langle v_f\rangle$. At Selke, the upper range of v_{f_water}, defined by the 95% confidence interval, exceeded $\langle v_f\rangle$ by roughly an order of magnitude in both seasons (Table 3; v_{f_water} published in Risse-Buhl et al. 2020*b*).

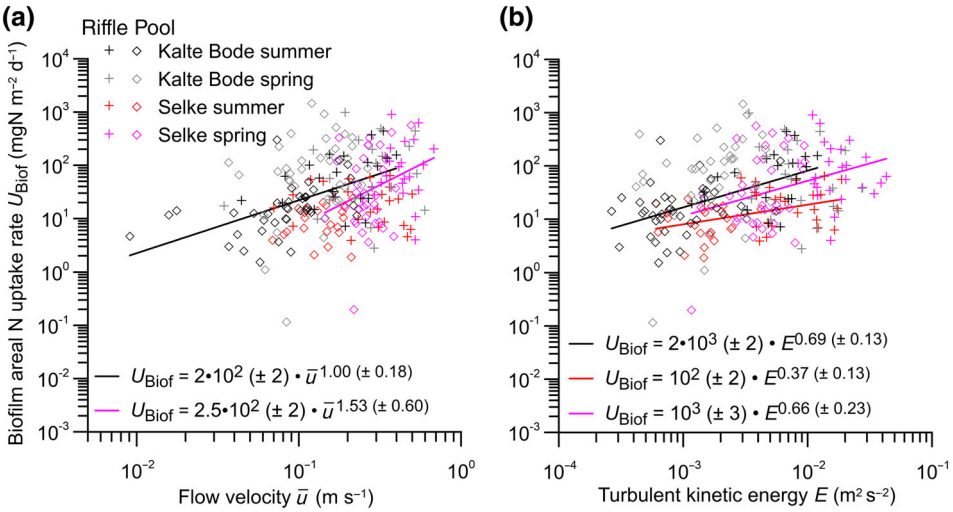

Fig. 3. Biofilm areal N uptake rate (U_{Biof}) as a function of flow velocity ($\bar{u}$) (**a**) and turbulent kinetic energy (**b**) plotted on log–log scaled axes. Symbols show results of each measurement campaign with symbol color referring to stream and season and symbol type referring to habitat. Solid lines show linear regressions for statistically significant relationships ($p < 0.05$). Regression equation including standard errors of the parameters in parenthesis is shown in the lower part of the panel.

Calculation of biofilm N uptake velocities (v_{bed}) resulted in a few negative values, mainly in Kalte Bode in summer with one third of all v_{bed} values being negative. For Kalte Bode in spring we calculated five, for Selke in spring one, and for Selke in summer no negative values were found (Table 1). Compared to k, the spatial average of the biofilm uptake velocity ($\langle v_{bed} \rangle$) was almost twice as high in Kalte Bode in summer, but much lower for all other campaigns. In particular, in Selke in summer, $\langle v_{bed} \rangle$ was 25 times lower than k. Thus, the overall uptake velocity $\langle V \rangle$ was comparable to $\langle V_{Biof} \rangle$ in Kalte Bode in spring and Selke in summer, but approximately twice as high in Selke in spring and 1.5 times higher in Kalte Bode in summer (Table 1).

Similar to hydraulic parameters but contrary to $\langle DM \rangle$, $\langle U_{Biof} \rangle$ and $\langle v_f \rangle$ tended to be higher in riffles than in pools for both streams and seasons. However, significant differences between riffles and pools could only be observed for Selke in summer (Table S2 in Supporting Information).

Hydraulic and biological controls on biofilm N uptake

The magnitude of near-bed flow had a stimulating effect on N uptake at the spot-scale in both streams and seasons. For example, U_{Biof} was positively related to E with an explanatory power of 32% ($p < 0.001$) for Kalte Bode in summer and 16% ($p = 0.006$) and 13% ($p = 0.006$) for Selke in summer and spring, respectively (Fig. 3b). Moreover, flow velocity ($\bar{u}$) significantly explained variability in biofilm areal N uptake rate for Kalte Bode in summer ($R^2 = 0.35$, $p < 0.001$) and Selke in spring ($R^2 = 0.10$, $p = 0.012$) (Fig. 3a).

The overall N uptake velocity of biofilms was significantly positively related to k across streams and seasons (Fig. 4). The mean uptake efficiency $\langle v_f/k \rangle$ sensu Grant et al. (2018*a*) was lower at Selke (spring: 4%, $R^2 = 0.31$, $p < 0.001$, summer: 14%, $R^2 = 0.60$, $p < 0.001$) than at Kalte Bode (spring: 23%, $R^2 = 0.24$, $p < 0.001$, summer: 140%, $R^2 = 0.40$, $p < 0.001$; Fig. 4). No differences were found between riffles and pools, except for Kalte Bode in spring, were pools showed higher N uptake velocities than riffles (Table S3 in Supporting Information).

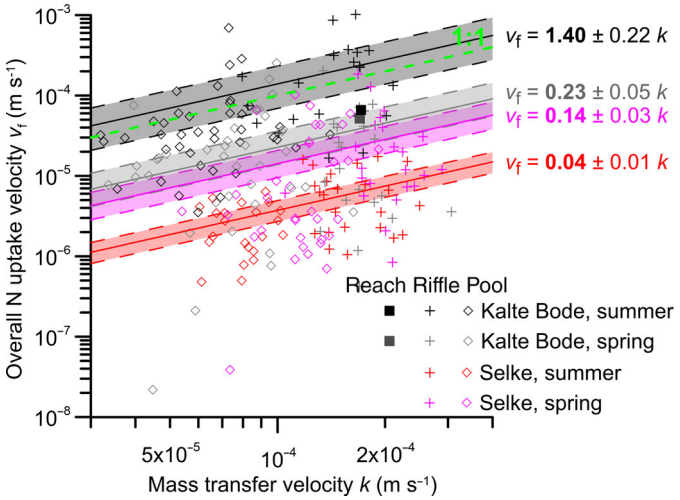

Fig. 4. Overall N uptake velocity (v_f) as a function of mass transfer velocity (k) plotted on log–log scaled axes. Symbols show results from each measurement campaign with symbol color referring to stream and season and symbol type referring to habitat. The solid lines show the linear fit through the origin with regression equations including standard error of the slope written next to the fitted lines. The dashed green line shows a 1 : 1 relationship. Dashed lines around the shaded areas delineate the 95% confidence interval for each measurement campaign. v_f for the reach-scale for Kalte Bode are taken from a companion study of Risse-Buhl et al. (2020*b*).

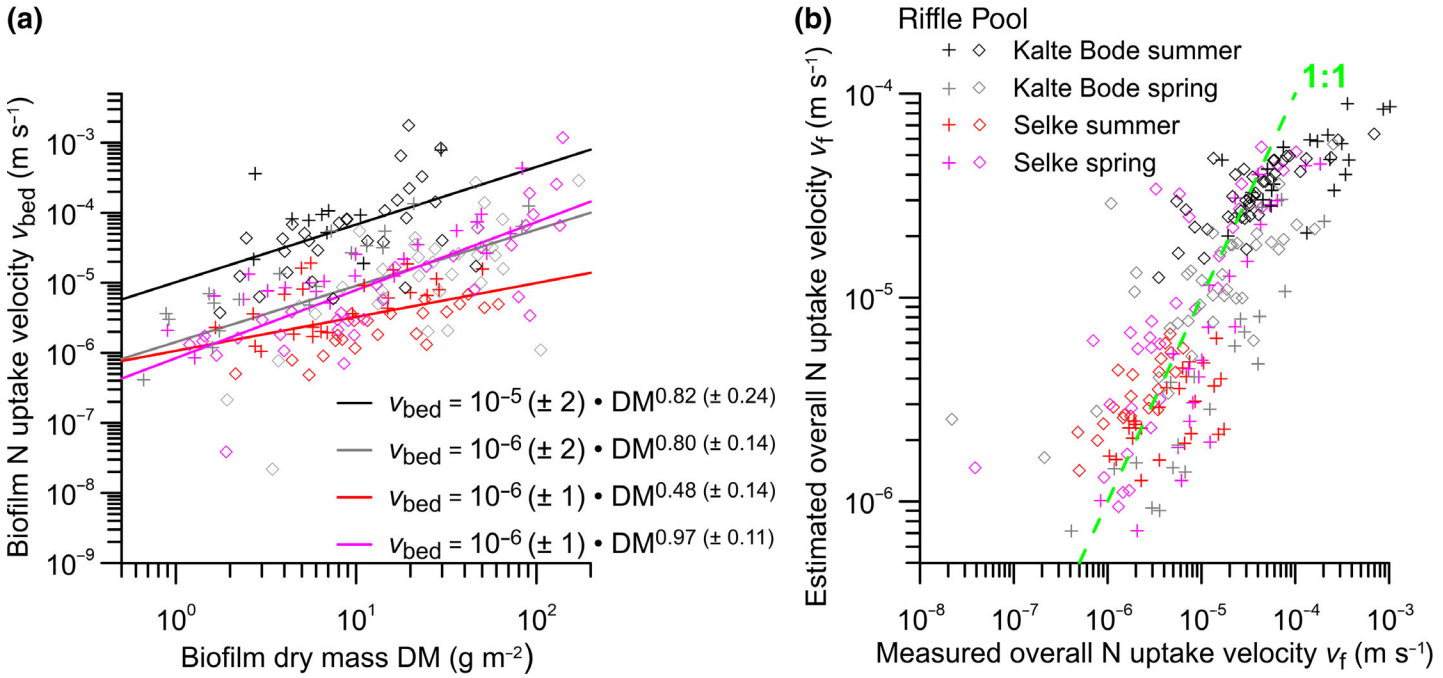

Fig. 5. (**a**) Biofilm N uptake velocity (v_{bed}) as a function of biofilm dry mass (DM) and (**b**) overall N uptake velocity (v_f) predicted from both, DM (from regression equations in (**a**)) and mass transfer velocity vs. observed overall N uptake velocity in ^{15}N tracer field studies plotted on log–log scaled axes. Symbols show results from each measurement campaign with symbol color referring to stream and season and symbol type referring to habitat. The solid lines in (**a**) show the linear fit with regression equations including standard errors of the parameters in parenthesis written next to the fitted lines. The dashed green line in (**b**) shows a 1 : 1 relationship.

The biologically mediated biofilm uptake velocity (v_{bed}; Eq. 8) was significantly positively related to biofilm dry mass for all streams and seasons (Fig. 5a). The explanatory power of biofilm dry mass obtained from linear regression ranged between 61% (Selke, $v_{bed} = 10^{-6}\,DM^{0.97}$, $p < 0.001$) and 38% (Kalte Bode, $v_{bed} = 10^{-6}\,DM^{0.80}$, $p < 0.001$) in spring and between 24% (Kalte Bode, $v_{bed} = 10^{-5}\,DM^{0.82}$, $p = 0.001$) and 22% (Selke, $v_{bed} = 10^{-6}\,DM^{0.48}$, $p = 0.001$) in summer (Fig. 5a). However, biofilm dry mass did not show a consistent relationship with flow parameters and was negatively related to E and $\overline{u}$ in Kalte Bode in spring, whereas it was related exclusively to $\overline{u}$ in Selke in summer (Fig. S2 in Supporting Information).

The estimated overall N uptake velocities were calculated from Eq. 8 with v_{bed} predicted from DM (Fig. 5a) and k. Results agreed well with the ^{15}N tracer field results of the overall N uptake velocities ($R^2 = 0.64$, $p < 0.001$, SE = 0.745), suggesting that N uptake processes can be broadly described in terms of two simple parameters: hydraulic conditions close to the sediment–water interface and biofilm biomass (Fig. 5b).

Discussion

Hydraulic control on N uptake

Our measurements in two gravel-bed streams with different nutrient background during two seasons revealed high spatial heterogeneity of areal N uptake rate of biofilms (U_{Biof}) and overall N uptake velocity (v_f) at the spot-scale. This heterogeneity was associated with spatial variability in hydraulic conditions and biofilm biomass. For example, the mean variability (i.e., standard deviation) of the turbulent dissipation rate (ε) within the experimental stream reaches exceeded the variability between the stream reaches by up to three times. The majority of the biogeochemical and hydraulic within-stream variability was furthermore related to mesoscale hydromorphological habitats (i.e., riffles and pools). Riffles were characterized by higher flow velocity ($\overline{u}$) and turbulent kinetic energy (E) and exceeded biofilm areal N uptake rates in pools, extending the findings from previous studies (Peipoch et al. 2016; Risse-Buhl et al. 2020*b*).

At the spot-scale, areal N uptake rate of biofilms increased with either $\overline{u}$, E, or both, except for Kalte Bode in spring. These observations imply that biofilm areal N uptake rate predominantly increased with increasing flow velocity and turbulence in both streams. Similar positive effects of flow velocity on benthic nutrient uptake have been observed in flume experiments (Battin et al. 2003*b*; Arnon et al. 2013; Roche et al. 2019) and in natural streams (Peipoch et al. 2016; Grant et al. 2018*a*). Natural streams exhibit wide ranges of streambed roughness, which determine flow and turbulence and its variability (Noss and Lorke 2016). This variability is reflected in the high variability of the mean flow velocity and the turbulent kinetic energy within our study reaches. Based

on the simultaneous measurement of hydraulics and N uptake, we show that hydraulic conditions created a biogeochemical mosaic characterized by hot and cold spots of biofilm N uptake. However, while $\overline{u}$ and E integrate hydraulic conditions, they can only indirectly infer turbulence-mediated mass transfer processes at the benthic interface.

The mass transfer velocity (k) describes the maximum, physically driven N uptake of the streambed (Grant et al. 2018*a*). At the spot-scale, k depends on ε and the Schmidt number (Sc) of the transported substance, assuming that mass transport is governed by boundary-layer turbulence (Lorke and Peeters 2006). Surface renewal theory in combination with the small eddy model has so far been applied for quantifying air–water gas transfer (Katul and Liu 2017; Lorke et al. 2019) but not to examine transfer processes at the benthic interface. Application of this approach in our study streams resulted in mass transfer velocities very well within the range of other studies. For example, $k/Sc^{-0.5}$ ranged from 10^{-3} to 10^{-4} m s^{-1} in our study, which coincides with values gathered in Lorke and Peeters (2006) for the sediment–water and water–air interface calculated from bed shear stress. Moreover, the mean mass transfer velocity in this study calculated from 230 flow measurements in both streams and seasons was precisely in the range of a study by Lorke et al. (2019), who presented mass transfer velocities across the air–water interface in streams for a similar range of Schmidt numbers ($570 < Sc > 660$ in our study). Similar to $\overline{u}$ and E, the mass transfer velocity among spots was highly variable, especially in Kalte Bode in spring, where it ranged over almost one order of magnitude. For comparison, in Grant et al. (2018*a*), the k calculated for 72 stream reaches across several biomes ranged over 1.5 orders of magnitude. On the mesoscale, we observed significantly higher k in riffles of both streams and seasons underlining the importance of direct hydraulic effects via mass transfer.

By deploying the surface renewal theory, we showed that hydraulic conditions directly translated into hydraulic mass transfer at the spot-scale at the benthic interface via ε. Surface renewal theory is applicable to the spatial scale of turbulent eddies. Grant et al. (2018*a*) estimated k from reach-scale dissipation rates (i.e., channel geometry, bed slope, and discharge). This approach assumes uniform flow conditions along the reach and does not resolve the high variability at the spot-scale, which can only be analyzed via local turbulence measurements. We show that surface renewal theory based on scales of the smallest turbulent eddies can be applied at the benthic interface and can be extrapolated to larger scales by spatial averaging.

The scaling factor α_1 (Eq. 3) depends on the distance of the flow measurement to the streambed because ε decreases reciprocally with distance from the streambed and relatively large variability is possible (Lorke and Peeters 2006; Esters et al. 2017). In marine environments, for example, uncertainties of α_1 can reach a factor of two (Tokoro et al. 2008). In this study, it is likely that most of the hydraulic measurements were conducted in the roughness sublayer, which is characterized by local form-induced flow and dispersion processes (Nikora 2010). Under these conditions, the assumptions underlying the calculation of transfer velocities from ε (Eq. 3) may not be directly applicable. Instead, sweep-ejection motions, which were also considered in Grant's expression of k, dominate transfer processes (O'Connor and Hondzo 2008). Comparison to this approach at the mesoscale would result in α_1 of 1.4 (Fig. S3 in Supporting Information). However, due to multiple measurements at similar heights above the bed, Eq. 3 was applied in analogy to the double-averaging procedure of the Navier–Stokes equation for the transfer of momentum in the roughness sublayer (Nikora et al. 2007). All measurements and samplings were conducted at discharges between baseflow and mean discharge. However, during the campaigns, we could not prevent changes in discharge, which decreased after the hydraulic measurements and was almost half of the discharge during the tracer experiment for Selke in summer and spring. Assuming a linear relation to bottom shear velocity (Lorke and Peeters 2006) and deductively from discharge, it can be estimated that mass transfer velocities varied by a factor of 2, which is comparable to the difference between riffles and pools. In summary, our study approach showed two limitations, both affecting the mass transfer velocity: the effects of varying discharge and the choice of α_1 are of importance when discussing uptake efficiencies. However, results from deploying the model in Eq. 8 and subsequent correlation with dry mass (Fig. 5b) are not affected because relating factors (i.e., slopes) would not change. Nevertheless, we suggest future studies should focus on measuring closer to the streambed using advanced techniques such as field-deployable particle image velocimetry (Lorke et al. 2019).

Biological control of N uptake

Despite high within-stream variability of biofilm dry mass, we demonstrated that the biologically mediated component of the overall N uptake velocity (i.e., biofilm uptake velocity v_{bed}) was positively correlated to biofilm dry mass for all streams and seasons. This positive relation between biofilm N uptake velocity and biomass might reach an equilibrium in eutrophic streams because extensive biofilm biomass can be a limiting factor for mass transfer within the biofilm matrix where nutrient availability decreases toward the biofilm base (De Beer et al. 1996). However, inactive biofilm biomass accumulating at the biofilm base as consequence of nutrient limitation is prone to detachment (Larned 2010; Machineni et al. 2017). An indirect effect of hydraulics on N uptake via biofilm biomass was evident at one out of four campaigns (Kalte Bode in spring), where higher $\overline{u}$ and E were associated with lower biofilm biomass. In a companion study in the same streams and seasons, we showed that biofilms became more compact with increasing turbulent kinetic energy by maintaining a comparable biofilm biomass per area (Risse-Buhl et al. 2017). This compact biofilm growth seemed to be

advantageous for resisting hydrodynamic shear forces in order to avoid displacement and for maintaining high N uptake. Besides biofilm biomass, hydrodynamic shear forces modulate biofilm community structure (Besemer et al. 2009; Singer et al. 2010; Risse-Buhl et al. 2020*a*), which indirectly can control biofilm N uptake (Cardinale 2011).

Stream biofilms are subjected to various kinds of disturbances (e.g., grazing, mechanical disturbance; Graba et al. 2014; Marcus et al. 2014). Disturbances can result in coexistence of biofilms of different successional stages and might explain the inconsistent effects of flow on biofilm biomass. Biomass additionally depends on the successional stage of biofilms with strongest effects of near-bed flow at intermediate successional stages (Besemer et al. 2007). The regulation of biofilm biomass at the spot-scale, however, is still difficult to predict and needs further experimental investigations, ideally coupled with dynamic biofilm community modeling.

Effects of environmental conditions and variability on biofilm N uptake

The ratio between overall N uptake velocity and mass transfer velocity (uptake efficiency sensu Grant et al. 2018*a*) is a measure of the relative importance of hydraulic and biological controls. A ratio near unity indicates that nutrient uptake is solely limited by mass transfer in the turbulent boundary layer, while a smaller ratio suggests increasing limitation by the uptake capacity of the biofilms. In our study, the uptake efficiency was mostly smaller than unity, indicating that both mass transfer and biological activity contributed to the spatial variability of areal N uptake rates. In general, uptake efficiencies were higher in the Kalte Bode as compared to the Selke with lowest values for the Selke in summer. The differences in uptake efficiencies between both streams coincided with different nutrient concentrations, which were lower in Kalte Bode. Higher uptake efficiencies in streams with lower nutrient background were also reported in Grant et al. 2018*a*. Furthermore, Grant et al. (2018*a*) reported a threshold of nitrate concentrations (10^{-3} mol m^{-3}) below which uptake is controlled by processes at or within the streambed rather than by mass transfer to the streambed. Nitrate concentrations in our two study streams were one order of magnitude larger (10^{-2} mol m^{-3}) than this threshold. This supports our result that mass transfer strongly affected biofilm areal N uptake rates. We are aware that ammonia uptake as investigated in this study is generally higher as compared to nitrate (Ribot et al. 2013), this may, in part, affect the comparison to Grant et al. (2018*a*).

Furthermore, biofilm biomass was subjected to seasonal changes of environmental conditions. For example, biofilm biomass was lower in summer most likely due to riparian shading and could have affected areal N uptake rates. Interestingly, in Kalte Bode in summer, uptake efficiencies were higher and varied around units, indicating that hydraulic control was more important (i.e., limiting) than biofilm dry mass. On the contrary to the presumptive positive effect of light on biofilm biomass and ultimately on areal N uptake rates, we could not find any effect of stream water temperature. Water temperature in Selke in summer was 6–7°C higher than in the other experiments but did not result in an increase of biofilm N uptake velocities. In summary, our results indicate that seasonally and hydrologically changing environmental conditions modulate the relevance of hydraulic and biological controls on N uptake.

Conclusions

Combined measurements of biofilm N uptake and hydraulic conditions in two gravel-bed streams of contrasting nutrient background revealed uptake rates were controlled by both, hydraulic (i.e., via mass transfer) and biological (i.e., via biofilm characteristics) mechanisms. Spatial variability of the turbulent dissipation rates and biofilm biomass explained the high within-stream heterogeneity of biofilm N assimilation. High flow heterogeneity can additionally foster other biological patterns not considered in this study but relevant for nutrient cycling. For example, local flow conditions have a substantial effect on biofilm diversity, architecture, and trophic interactions (Risse-Buhl et al. 2017, 2020*a*). It remains unclear as to whether these parameters explain unaccounted variance of our measured N uptake rates and needs to be elaborated in future studies.

We found that spatially averaged turbulent dissipation rates and resulting mass transfer velocities measured at the spot-scale agreed well with values predicted from hydromorphological bulk properties. Beyond the reach-scale, it can be expected that the calculation of the mass transfer velocity by averaging bulk parameters can be extended to scales of many kilometers and up to the river network scale; however, this requires confirmation by future studies. We suggest that prospective research should additionally include the effects of permeable sediments and hyporheic exchange (see also Grant et al. 2018*b*). In conclusion, the knowledge of processes at small spatial scales will prompt our understanding of the functioning of stream ecosystems at larger spatial scales and supports upscaling to larger spatiotemporal scales along stream networks.

Authors contribution

All authors came up with the research questions and designed the study approach. CA, URB, DvS and CN performed the research, CA, DvS, CN and AL analyzed the data, and CA and AL wrote the paper with comments from URB, DvS, CN and MW.

Data Availability Statement

The data that support the findings of this study are available from the corresponding author upon request.

References

Alexander, R. B., E. W. Boyer, R. A. Smith, G. E. Schwarz, and R. B. Moore. 2007. The role of headwater streams in downstream water quality. J. Am. Water Resour. Assoc. **43**: 41–59. doi:10.1111/j.1752-1688.2007.00005.x

Arnon, S., K. Yanuka, and A. Nejidat. 2013. Impact of overlying water velocity on ammonium uptake by benthic biofilms. Hydrol. Process. **27**: 570–578. doi:10.1002/hyp.9239

Battin, T. J., L. A. Kaplan, J. D. Newbold, X. Cheng, and C. Hansen. 2003*a*. Effects of current velocity on the nascent architecture of stream microbial biofilms. Appl. Environ. Microbiol. **69**: 5443–5452. doi:10.1128/aem.69.9.5443-5452.2003

Battin, T. J., L. A. Kaplan, J. D. Newbold, and C. M. E. Hansen. 2003*b*. Contributions of microbial biofilms to ecosystem processes in stream mesocosms. Nature **426**: 439–442. doi:10.1038/nature02152

Battin, T. J., W. T. Sloan, S. Kjelleberg, H. Daims, I. M. Head, T. P. Curtis, and L. Eberl. 2007. Microbial landscapes: New paths to biofilm research. Nat. Rev. Microbiol. **5**: 76–81. doi:10.1038/nrmicro1556

Besemer, K., G. A. Singer, I. Hödl, and T. J. Battin. 2009. Bacterial community composition of stream biofilms in spatially variable-flow environments. Appl. Environ. Microbiol. **75**: 7189–7195. doi:10.1128/aem.01284-09

Besemer, K., G. A. Singer, R. Limberger, A.-K. Chlup, G. Hochedlinger, I. Hödl, C. Baranyi, and T. J. Battin. 2007. Biophysical controls on community succession in stream biofilms. Appl. Environ. Microbiol. **73**: 4966–4974. doi:10.1128/aem.00588-07

Biggs, B. J. F., and H. A. Thomsen. 1995. Disturbance of stream periphyton by perturbations in shear stress: Time to structural failure and differences in community resistance. J. Phycol. **31**: 233–241. doi:10.1111/j.0022-3646.1995.00233.x

Bluteau, C. E., N. L. Jones, and G. N. Ivey. 2011. Estimating turbulent kinetic energy dissipation using the inertial subrange method in environmental flows. Limnol. Oceanogr.: Methods **9**: 302–321. doi:10.4319/lom.2011.9.302

Brand, A., C. Noss, C. Dinkel, and M. Holzner. 2016. High-resolution measurements of turbulent flow close to the sediment–water interface using a bistatic acoustic profiler. J. Atmos. Ocean. Technol. **33**: 769–788. doi:10.1175/JTECH-D-15-0152.1

Buffin-Bélanger, T., and A. G. Roy. 2005. 1 min in the life of a river: Selecting the optimal record length for the measurement of turbulence in fluvial boundary layers. Geomorphology **68**: 77–94. doi:10.1016/j.geomorph.2004.09.032

Cardinale, B. J. 2011. Biodiversity improves water quality through niche partitioning. Nature **472**: 86–89. doi:10.1038/nature09904

Day, T. J. 1977. Observed mixing lengths in mountain streams. J. Hydrol. **35**: 125–136. doi:10.1016/0022-1694(77)90081-6

De Beer, D., P. Stoodley, and Z. Lewandowski. 1996. Liquid flow and mass transport in heterogeneous biofilms. Water Res. **30**: 2761–2765. doi:10.1016/S0043-1354(96)00141-8

Esters, L., S. Landwehr, G. Sutherland, T. G. Bell, K. H. Christensen, E. S. Saltzman, S. D. Miller, and B. Ward. 2017. Parameterizing air-sea gas transfer velocity with dissipation. J. Geophys. Res. Ocean. **122**: 3041–3056. doi:10.1002/2016JC012088

Frissell, C. A., W. J. Liss, C. E. Warren, and M. D. Hurley. 1986. A hierarchical framework for stream habitat classification: Viewing streams in a watershed context. Environ. Manag. **10**: 199–214.

Galloway, J. N., and others. 2008. Transformation of the nitrogen cycle: Recent trends, questions, and potential solutions. Science **320**: 889–892. doi:10.1126/science.1136674

Goring, D. G., and V. Nikora. 2002. Despiking acoustic Doppler velocimeter data. J. Hydraul. Eng. **128**: 117–126. doi:10.1061/(ASCE)0733-9429(2002)128:1(117)

Graba, M., and others. 2014. Modelling epilithic biofilms combining hydrodynamics, invertebrate grazing and algal traits. Freshw. Biol. **59**: 1213–1228. doi:10.1111/fwb.12341

Grant, S. B., M. Azizian, P. Cook, F. Boano, and M. A. Rippy. 2018*a*. Factoring stream turbulence into global assessments of nitrogen pollution. Science **359**: 1266–1269. doi:10.1126/science.aap8074

Grant, S. B., J. D. Gomez-Velez, and M. Ghisalberti. 2018*b*. Modeling the effects of turbulence on hyporheic exchange and local-to-global nutrient processing in streams. Water Resour. Res. **54**: 5883–5889. doi:10.1029/2018WR023078

Grant, S. B., and I. Marusic. 2011. Crossing turbulent boundaries: Interfacial flux in environmental flows. Environ. Sci. Technol. **45**: 7107–7113. doi:10.1021/es201778s

Holmes, R. M., J. W. McClelland, D. M. Sigman, B. Fry, and B. J. Peterson. 1998. Measuring ^{15}N-NH_4^+ in marine, estuarine and fresh waters: An adaptation of the ammonia diffusion method for samples with low ammonium concentrations. Mar. Chem. **60**: 235–243. doi:10.1016/S0304-4203(97)00099-6

Katul, G., and H. Liu. 2017. Multiple mechanisms generate a universal scaling with dissipation for the air-water gas transfer velocity. Geophys. Res. Lett. **44**: 1892–1898. doi:10.1002/2016GL072256

Kim, B. K. A., A. P. Jackman, and F. J. Triska. 1992. Modeling biotic uptake by periphyton and transient hyporrheic storage of nitrate in a natural stream. Water Resour. Res. **28**: 2743–2752.

Koca, K., C. Noss, C. Anlanger, A. Brand, and A. Lorke. 2017. Performance of the Vectrino Profiler at the sediment–water interface. J. Hydraul. Res. **55**: 573–581. doi:10.1080/00221686.2016.1275049

Lamarre, H., and A. G. Roy. 2005. Reach scale variability of turbulent flow characteristics in a gravel-bed river. Geomorphology **68**: 95–113. doi:10.1016/j.geomorph.2004.09.033

Larned, S. T. 2010. A prospectus for periphyton: Recent and future ecological research. J. North Am. Benthol. Soc. **29**: 182–206. doi:10.1899/08-063.1

Larned, S. T., V. Nikora, and B. J. F. Biggs. 2004. Mass-transfer-limited nitrogen and phosphorus uptake by stream

periphyton: A conceptual model and experimental evidence. Limnol. Oceanogr. **49**: 1992–2000. doi:10.4319/lo.2004.49.6.1992

Lorke, A., P. Bodmer, K. Koca, and C. Noss. 2019. Hydrodynamic control of gas-exchange velocity in small streams. EarthArXiv. doi:10.31223/osf.io/8u6vc

Lorke, A., and F. Peeters. 2006. Toward a unified scaling relation for interfacial fluxes. J. Phys. Oceanogr. **36**: 955–961. doi:10.1175/JPO2903.1

Machineni, L., A. Rajapantul, V. Nandamuri, and P. D. Pawar. 2017. Influence of nutrient availability and quorum sensing on the formation of metabolically inactive microcolonies within structurally heterogeneous bacterial biofilms: An individual-based 3D cellular automata model. Bull. Math. Biol. **79**: 594–618. doi:10.1007/s11538-017-0246-9

Marcé, R., D. von Schiller, R. Aguilera, E. Martí, and S. Bernal. 2018. Contribution of hydrologic opportunity and biogeochemical reactivity to the variability of nutrient retention in river networks. Global Biogeochem. Cycles **32**: 376–388. doi:10.1002/2017GB005677

Marcus, H., J. K. Wey, H. Norf, and M. Weitere. 2014. Disturbance alters the response of consumer communities towards warming: A mesocosm study with biofilm-dwelling ciliates. Ecosphere **5**: art10. doi:10.1890/ES13-00170.1

Montgomery, D. R., and J. M. Buffington. 1997. Channel reach morphology in moutain drainage basins. Geol. Soc. Am. Bull. **109**: 596–611.

Moog, D. B., and G. H. Jirka. 1999. Air-water gas transfer in uniform channel flow. J. Hydraul. Eng. **125**: 3–10. doi:10.1061/(ASCE)0733-9429(1999)125:1(3)

Mulholland, P. J., J. L. Tank, D. M. Sanzone, W. M. Wollheim, B. J. Peterson, J. R. Webster, and J. L. Meyer. 2000. Nitrogen cycling in a forest stream determined by a 15 N tracer addition. Ecol. Monogr. **70**: 471. doi:10.2307/2657212

Nepf, H. M. 2011. Flow over and through biota, p. 267–288. *In* E. Wolanski and D. McLusky [eds.], Treatise on estuarine and coastal science. Elsevier Inc.

Newbold, J. D., R. V. O'Neill, J. W. Elwood, and W. Van Winkle. 1982. Nutrient spiralling in streams: Implications for nutrient limitation and invertebrate activity. Am. Nat. **120**: 628–652.

Nikora, V. 2010. Hydrodynamics of aquatic ecosystems: An interface between ecology, biomechanics and environmental fluid mechanics. River Res. Appl. **26**: 367–384. doi:10.1002/rra.1291

Nikora, V., D. G. Goring, and B. J. F. Biggs. 2002. Some observations of the effects of micro-organisms growing on the bed of an open channel on the turbulence properties. J. Fluid Mech. **450**: 317–341. doi:10.1017/s0022112001006486

Nikora, V., I. McEwan, S. McLean, S. Coleman, D. Pokrajac, and R. Walters. 2007. Double-averaging concept for rough-bed open-channel and overland flows: Theoretical background. J. Hydraul. Eng. **133**: 873–883. doi:10.1061/(asce)0733-9429(2007)133:8(873)

Noss, C., and A. Lorke. 2016. Roughness, resistance, and dispersion: Relationships in small streams. Water Resour. Res. **52**: 2802–2821. doi:10.1002/2015WR017449

O'Connor, B. L., and M. Hondzo. 2008. Dissolved oxygen transfer to sediments by sweep and eject motions in aquatic environments. Limnol. Oceanogr. **53**: 566–578. doi:10.4319/lo.2008.53.2.0566

Peipoch, M., E. Gacia, E. Bastias, A. Serra, L. Proia, M. Ribot, S. N. Merbt, and E. Martí. 2016. Small-scale heterogeneity of microbial N uptake in streams and its implications at the ecosystem level. Ecology **97**: 1329–1344. doi:10.1890/15-1210.1

Ribot, M., D. von Schiller, and E. Martí. 2017. Understanding pathways of dissimilatory and assimilatory dissolved inorganic nitrogen uptake in streams. Limnol. Oceanogr. **62**: 1166–1183. doi:10.1002/lno.10493

Ribot, M., D. von Schiller, M. Peipoch, F. Sabater, N. B. Grimm, and E. Martí. 2013. Influence of nitrate and ammonium availability on uptake kinetics of stream biofilms. Freshw. Sci. **32**: 1155–1167. doi:10.1899/12-209.1

Risse-Buhl, U., C. Anlanger, A. Chatzinotas, C. Noss, A. Lorke, and M. Weitere. 2020*a*. Near streambed flow shapes microbial guilds within and across trophic levels in fluvial biofilms. Limnol. Oceanogr. **65**: 2261–2277. doi:10.1002/lno.11451

Risse-Buhl, U., C. Anlanger, K. Kalla, T. R. Neu, C. Noss, A. Lorke, and M. Weitere. 2017. The role of hydrodynamics in shaping the composition and architecture of epilithic biofilms in fluvial ecosystems. Water Res. **127**: 211–222. doi:10.1016/j.watres.2017.09.054

Risse-Buhl, U., C. Anlanger, C. Noss, A. Lorke, D. von Schiller, and M. Weitere. 2020*b*. Hydromorphologic sorting of in-stream nitrogen uptake across spatial scales. Ecosystems **24**: 1184–1202. doi:10.1007/s10021-020-00576-7

Roche, K. R., A. J. Shogren, A. F. Aubeneau, J. L. Tank, and D. Bolster. 2019. Modeling benthic versus hyporheic nutrient uptake in unshaded streams with varying substrates. J. Geophys. Res. Biogeosci. **124**: 367–383. doi:10.1029/2018JG004684

Sabater, S., H. Guasch, A. M. Romani, and I. Munoz. 2002. The effect of biological factors on the efficiency of river biofilms in improving water quality. Hydrobiologia **469**: 149–156. doi:10.1023/a:1015549404082

Schindelin, J., and others. 2012. Fiji: An open-source platform for biological-image analysis. Nat. Methods **9**: 676–682. doi:10.1038/nmeth.2019

Seitzinger, S. P., and others. 2010. Global river nutrient export: A scenario analysis of past and future trends. Global Biogeochem. Cycles **24**. doi:10.1029/2009gb003587

Singer, G. A., K. Besemer, P. Schmitt-Kopplin, I. Hodl, and T. J. Battin. 2010. Physical heterogeneity increases biofilm resource use and its molecular diversity in stream mesocosms. PLoS One **5**: e9988. doi:10.1371/journal.pone.0009988

Stevenson, R. J. 1996. The stimulation and drag of current, p. 321–340. *In* R. J. Stevenson, M. L. Bothwell, and R. L. Lowe [eds.], Algal ecology: Freshwater benthic ecosystems. Academic Press.

Stoodley, P., I. Dodds, J. D. Boyle, and H. M. Lappin-Scott. 1998. Influence of hydrodynamics and nutrients on biofilm structure. J. Appl. Microbiol. **85**: 19S–28S. doi:10.1111/j.1365-2672.1998.tb05279.x

Tank, J. L., and others. 2018. Partitioning assimilatory nitrogen uptake in streams: An analysis of stable isotope tracer additions across continents. Ecol. Monogr. **88**: 120–138. doi:10.1002/ecm.1280

Tokoro, T., H. Kayanne, A. Watanabe, K. Nadaoka, H. Tamura, K. Nozaki, K. Kato, and A. Negishi. 2008. High gas-transfer velocity in coastal regions with high energy-dissipation rates. J. Geophys. Res. **113**: C11006. doi:10.1029/2007JC004528

Tomasek, A. A., T. D. Barman, P. Wang, J. L. Kozarek, C. Staley, M. J. Sadowsky, and M. Hondzo. 2018. The effects of turbulence and carbon amendments on nitrate uptake and microbial gene abundances in stream sediment. J. Geophys. Res. Biogeosci. **123**: 1289–1301. doi:10.1002/2017JG004261

Vogel, S. 1994. Life in moving fluids: The physical biology of flow, 2nd ed. Princeton Univ. Press.

von Schiller, D., E. MartÍ, J. L. Riera, and F. Sabater. 2007. Effects of nutrients and light on periphyton biomass and nitrogen uptake in Mediterranean streams with contrasting land uses. Freshw. Biol. **52**: 891–906. doi:10.1111/j.1365-2427.2007.01742.x

Wahl, T. L. 2003. Discussion of "Despiking Acoustic Doppler Velocimeter Data" by Derek G. Goring and Vladimir I. Nikora. J. Hydraul. Eng. **129**: 484–487. doi:10.1061/(ASCE)0733-9429(2003)129:6(484)

Weitere, M., and others. 2018. The food web perspective on aquatic biofilms. Ecol. Monogr. **88**: 543–559. doi:10.1002/ecm.1315

Wollschläger, U., and others. 2017. The Bode hydrological observatory: A platform for integrated, interdisciplinary hydro-ecological research within the TERENO Harz/Central German Lowland Observatory. Environ. Earth Sci. **76**: 29. doi:10.1007/s12665-016-6327-5

Acknowledgments

We are grateful to P. Portius and his team for technical support as well as S. Bauth, B. Bayer, M. Diener, S. Geisthard, H. Goreczka, S. Halbedel, K. Kalla, N. Kamjunke, U. Kiwel, B. Kuehn, U. Kuhlicke, V. Kunz, K. Lerche, U. Link, I. Locker, C. Mendoza-Lera, H. Norf, N. Oberhoffner, L. Parlow, C. Seiler, I. Siebert, U. Strachauer, M. Vieweg, N. Wells, K. Westphal, R. Wild, and F. Zander for their invaluable help during the field campaigns. We thank M. Brauns for field assistance and discussions on data analysis and interpretation. J. Zubrod and B. Michener analyzed samples for stable isotopes of nitrogen. The research benefited from the TERENO (Terrestrial Environmental Observatories) infrastructure. The project was financed by research grants from the German Research Foundation (LO 1150/8-1 and WE 3545/6-1). D. von Schiller was a Serra Húnter Fellow and was additionally supported by the research group grant FORESTREAM from the Catalan Government (2017 SGR 976). Open Access funding enabled and organized by Projekt DEAL.

Conflict of Interest

None declared.

Submitted 01 October 2020
Revised 16 April 2021
Accepted 27 July 2021

Associate editor: Robert O. Hall, Jr.